



Chhantyal-Pun, R., Khan, M. A. H., Martin, R., Zachhuber, N., Buras, Z. J., Percival, C. J., Shallcross, D. E., & Orr-Ewing, A. J. (2019). Direct Kinetic and Atmospheric Modelling Studies of Criegee Intermediate Reactions with Acetone. *ACS Earth and Space Chemistry*, 3(10), 2363-2371.
<https://doi.org/10.1021/acsearthspacechem.9b00213>

Peer reviewed version

Link to published version (if available):
[10.1021/acsearthspacechem.9b00213](https://doi.org/10.1021/acsearthspacechem.9b00213)

[Link to publication record in Explore Bristol Research](#)
PDF-document

This is the author accepted manuscript (AAM). The final published version (version of record) is available online via ACS Publications at <https://pubs.acs.org/doi/10.1021/acsearthspacechem.9b00213>. Please refer to any applicable terms of use of the publisher.

University of Bristol - Explore Bristol Research

General rights

This document is made available in accordance with publisher policies. Please cite only the published version using the reference above. Full terms of use are available:
<http://www.bristol.ac.uk/red/research-policy/pure/user-guides/ebr-terms/>

Direct Kinetic and Atmospheric Modelling Studies of Criegee Intermediate Reactions with Acetone

Rabi Chhantyal-Pun†, M. Anwar H. Khan†, Rebecca Martin†, Nicholas Zachhuber†, Zachary J. Buras‡, Carl J. Percival||, Dudley E. Shallcross†, Andrew J. Orr-Ewing*†*

†School of Chemistry, University of Bristol, Cantock's Close, Bristol BS8 1TS, United

Kingdom, ‡Department of Chemical Engineering, Massachusetts Institute of Technology, 77

Massachusetts Avenue, Cambridge, Massachusetts 02139, USA, ||Jet Propulsion Laboratory,

California Institute of Technology, 4800 Oak Drive, Pasadena, CA 91109-8099, USA.

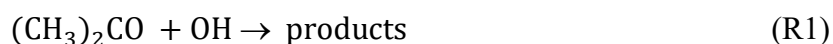
KEYWORDS: Criegee Intermediates, Acetone, Atmospheric Chemistry, Global Modelling, Reaction Rates

ABSTRACT: Mounting evidence suggests that Criegee intermediates are important tropospheric oxidants of both organic and inorganic gases, supplementing the oxidation chemistry initiated by OH radicals. Here, the rate coefficient for reaction of the simplest Criegee intermediate CH₂OO with acetone, $k(\text{CH}_2\text{OO} + (\text{CH}_3)_2\text{CO})$, was measured using laser flash photolysis and cavity ring-down spectroscopy methods under tropospherically relevant conditions of pressure and temperature. The pressure dependence of $k(\text{CH}_2\text{OO} + (\text{CH}_3)_2\text{CO}) = (4.7 \pm 0.1) \times 10^{-13} [\text{N}_2] / ((3.7 \pm 0.7) \times 10^{16} + [\text{N}_2]) \text{ cm}^3 \text{ molecule}^{-1} \text{ s}^{-1}$ was measured in the 5 to 100 Torr range, returning a high-pressure limit value of $(4.7 \pm 0.1) \times 10^{-13} \text{ cm}^3 \text{ molecule}^{-1} \text{ s}^{-1}$ at 293 K. A temperature dependence of $k(\text{CH}_2\text{OO} + (\text{CH}_3)_2\text{CO}) = (1.45 \pm 0.18) \times 10^{-21} \text{ T}^2 \exp(2407 \pm 36 / \text{T}) \text{ cm}^3 \text{ molecule}^{-1} \text{ s}^{-1}$ was observed in the 250 to 310 K range. The global chemical transport model (STOCHEM-CRI) was used to model the speciated Criegee intermediate field

using recently reported temperature dependent rate coefficient values for various reactions of Criegee intermediates. Incorporation of the Criegee intermediate reaction with acetone in the model predicts decreases in acetone concentration of as much as 10 to 40 ppt in various regions of the world.

1. Introduction

Acetone ((CH₃)₂CO) is emitted directly into the atmosphere by plants, or produced by photochemical oxidation of volatile organic compounds (VOCs) of anthropogenic (e.g., isopentane and isobutane) and biogenic (monoterpenes) origins.¹ Background mixing ratios of acetone in the troposphere up to 0.2 and 0.5 ppb have been reported in the southern and northern hemispheres, respectively.² Acetone is a source of acetyl radicals, which can react with oxygen and nitrogen dioxide to form peroxyacetylnitrate (PAN). Thus, PAN acts as a reservoir of NO_x, an important precursor to ozone in the lower atmosphere.³ The main atmospheric sinks of acetone are reaction with OH radical, photolysis, and dry deposition (reactions (R1) – (R3)), with an expected lifetime of 15-35 days.^{1, 3-5} Here, we consider the significance of reactions with Criegee intermediates, reaction (R4), as an additional loss process, most likely producing a secondary ozonide (SOZ).



Criegee intermediates are produced in the troposphere during the ozonolysis of alkenes.⁶ Many are removed by reaction with H₂O, (H₂O)₂ or unimolecular decomposition.^{7, 8} However,

certain Criegee intermediates such as syn-methyl vinyl oxide (syn-MVKOO), produced during the ozonolysis of isoprene, and others produced from pinenes, react only slowly with H₂O or (H₂O)₂ and have slow unimolecular rates of decomposition.^{9, 10} They are therefore expected to undergo bimolecular reactions with other trace gases in the troposphere. For example, Criegee intermediates can react with SO₂ to produce SO₃ and hence tropospheric H₂SO₄, an important precursor for aerosol formation in the troposphere.^{11, 12} Rates of reaction of Criegee intermediates with various inorganic and organic acids are near or above the collision limit, and are likely the dominant reactive sink of these acids in forested regions around the world.¹³⁻¹⁵ These reactions are expected to produce multi-functionalized organic hydroperoxides, which may also be important precursors for secondary organic aerosol in the troposphere.¹⁵ Recently, rate coefficients for reaction of the simplest Criegee intermediate, CH₂OO, with acetone (Reaction (R5)) have been measured using multiplexed photoionization mass spectrometry¹⁶ and ultraviolet absorption spectroscopy.¹⁷



The reaction rate exhibits a negative temperature dependence in the 298 K to 500 K range, and association of the two reactants was found to produce a secondary ozonide. A further kinetic study of the CH₂OO + (CH₃)₂CO reaction is presented here, with a focus on temperatures and pressures more relevant in the troposphere. The new data set is used to obtain a refined value for the reaction barrier height, using kinetic master equation (ME) calculations. Finally, global atmospheric chemistry modelling is performed to assess the impact of Criegee intermediate reactions with acetone in the troposphere.

2. Methods

2.1. Cavity Ring-Down Spectroscopy. Kinetic measurements of the $\text{CH}_2\text{OO} + (\text{CH}_3)_2\text{CO}$ reaction were performed using a laser flash photolysis method. In short, CH_2OO was produced by UV ($\lambda = 355 \text{ nm}$) photolysis of CH_2I_2 using the third harmonic of a Nd:YAG laser, in the presence of oxygen.¹⁸ Cavity ring-down spectroscopy (CRDS) was used to probe CH_2OO using its broad ultraviolet absorption band, with a chosen probe wavelength also of 355 nm. The probe radiation was generated by frequency doubling the visible radiation generated by a dye laser operating with pyridine II dye and pumped at 532 nm by the second harmonic of the fundamental output of a Nd:YAG laser. A temperature-controlled flow reactor coupled with a CRD spectrometer and photolysis laser was used to confine and monitor the formation of CH_2OO and its loss by reaction with acetone. Premixes were prepared of acetone diluted to known ratios in N_2 , and the chosen acetone/ N_2 mixture and the other gas samples used were introduced into the reactor through separate mass flow controllers. The partial pressures and concentrations of each gas were determined by multiplying their partial flow rates by calibration factors derived from the total gas flow rate and measurements of the total pressure, made close to the laser overlap region inside the reactor. Bimolecular rate coefficients values were measured as a function of temperature (250 to 310 K) and pressure (5 to 100 Torr) in a flowing mixture mostly comprising O_2 and N_2 . Further details of the spectrometer and the temperature-controlled flow reactor used have been reported previously.^{14, 19}

2.2. STOCHEM-CRI Model. STOCHEM (Stratospheric and Tropospheric Chemistry) is an offline chemical transport model which has been used in the past to study ozone chemistry in the troposphere.^{20, 21} The STOCHEM model adopts a Lagrangian approach in which 50000 constant mass air parcels are advected every three hours according to wind fields generated by the Meteorological Office global circular model. The meteorological parameterisations in STOCHEM have been described in previous papers.^{12, 22, 23} STOCHEM is coupled with the

CRI v2-R5 (common representative intermediate, version 2 reduction 5) scheme, which is a reduced chemical reaction scheme optimized in terms of ozone formation and can be used for efficient calculations in global modelling studies with reduced computational cost. The details of the CRI mechanism and its reduction mechanisms can be found in previous publications.²⁴⁻²⁶ Each Lagrangian air parcel accommodates individual concentrations of 229 species which compete in 530 chemical reactions.¹ Chemical processes occur within the air parcels in addition to emissions, depositions, convection and other removal processes of all species which are uncoupled from the advection. The global emissions of acetone originating from the surface (i.e. 0.297 Tg/yr for anthropogenic, 1.83 Tg/yr for biomass burning and 44.0 Tg/yr for vegetation) were added in the model as shown previously by Shallcross and co-workers.¹ In the current study, the CRI mechanism has been updated with the incorporation of explicit formation and loss processes of individual stabilized Criegee intermediates. The specific stabilized Criegee intermediates, and their losses included in the model are summarized in Table 1. Following the inclusion of the Criegee intermediates, each air parcel contains concentrations of a total of 246 species that compete in 578 chemical reactions. Using this new Criegee field, a simulation was conducted after including the reaction of acetone and Criegee intermediates to investigate the impact of Criegee intermediates on the reduction of tropospheric acetone levels. The simulation was conducted for 24 months, with the first 12 months allowing the model to spin up, and the analysis performed on the second 12 months of data.

3. Results and Discussion

3.1. Kinetics of $\text{CH}_2\text{OO} + (\text{CH}_3)_2\text{COO}$ reaction. Values of the bimolecular rate coefficient, k_5 , for the $\text{CH}_2\text{OO} + (\text{CH}_3)_2\text{CO}$ reaction were measured at different pressures and temperatures

using the pseudo first order method, in which the concentration of acetone was in excess. Under our experimental conditions, the decay rate of measured Criegee intermediate signal depends on the fast-self-reaction, and (pseudo) first order loss mainly attributable to reaction with excess co-reactants.^{19,27} The integrated rate expression of equation (E1) for simultaneous first and second order decay process was used to fit the CH₂OO decay traces.

$$\Delta\kappa(t) = \frac{k_p}{\frac{k_p}{\Delta\kappa(t_0)} e^{k_p t} - k' \left(\frac{2L}{cd}\right) + k' \left(\frac{2L}{cd}\right) e^{k_p t}} \quad (\text{E1})$$

Here, $\Delta\kappa$ is the change in ring-down rate with and without the photolysis laser beam, k_p is an overall pseudo first order loss rate coefficient, k' is the second order loss rate coefficient for self-reaction scaled by the absorption cross section of CH₂OO at the probe laser wavelength (355 nm), c is the speed of light, L is the length of the cavity and d is the overlap length of the photolysis and probe lasers. A detailed derivation for this expression, and description of the fitting procedure are provided in our previous publication.¹⁹ Figure 1 shows an example of the fit obtained using constrained values of k' from separate determinations under given pressure and temperature conditions, which returns k_p values for the decay traces obtained in the presence of various concentrations of acetone. The k_p values are linearly dependent on the acetone concentration, as is illustrated in the inset to Figure 1, and the gradient of a best-fit line gives the bimolecular rate coefficient for the CH₂OO + (CH₃)₂CO reaction at the pressure and temperature of the measurements. A systematic uncertainty of 2% was expected for acetone concentrations deriving from uncertainties in flow rate, temperature and pressure measurements. This uncertainty was propagated with the 1 σ statistical uncertainty of the fits to give the total error estimates.

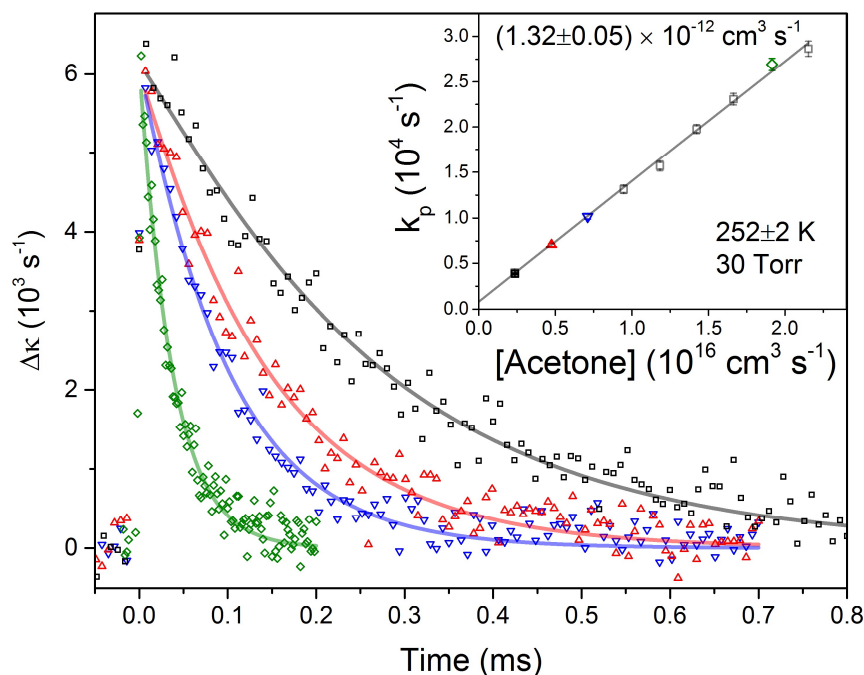
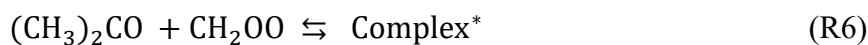


Figure 1. Representative example of the pseudo first order method for measurement of a bimolecular rate coefficient for reaction (R5). The coloured points show the CH₂OO decay traces obtained in the presence of various concentrations of acetone, and the solid lines are fits obtained using equation E1. The inset shows a plot of k_p values obtained from the fits as a function of acetone concentration, and the solid line is a linear fit to all the data points. The measurements were obtained at 30 Torr bath gas (mainly N₂) pressure and a temperature of 252 ± 2 K.

To explore the pressure dependence of the reaction rate, k_5 values were measured at various bath gas pressures and room temperature (293 K), as shown in Figure 2. The rate coefficient values are provided in Table S1 in the supporting information. The total pressure was increased by raising the flow rate of nitrogen gas while keeping the flow rates of all other reagent gases constant. The k_5 values suggest a weak pressure dependence from 5 to 30 Torr before reaching a constant value of around 4.6×10^{-13} cm³ molecule⁻¹ s⁻¹. A simple kinetic model assuming

stabilization of an association complex (reactions (R6) – (R8)) was used to fit the pressure dependent rate coefficients.



The fit expression of equation (E4) can be derived by applying the steady state approximation for the concentration of energized complex molecules (Complex*).

$$\frac{d[\text{Complex}^*]}{dt} = (k_6[(\text{CH}_3)_2\text{CO}][\text{CH}_2\text{OO}] - k_{-6}[\text{Complex}^*] - k_7[\text{Complex}^*][\text{M}] - k_8[\text{Complex}^*]) = 0 \quad (\text{E2})$$

$$k_5(\text{M}) = \frac{k_6(k_8 + k_7[\text{M}])}{k_{-6} + k_8 + k_7[\text{M}]} \quad (\text{E3})$$

If the rate of stabilisation is assumed to be much faster than the unimolecular reaction of the energized complex ($k_7[\text{M}] \gg k_8$), equation (E3) simplifies to

$$k_5(\text{M}) = \frac{k_6[\text{M}]}{k_{-6}/k_7 + [\text{M}]} \quad (\text{E4})$$

A similar model was used previously to explain the pressure dependence of the $(\text{CH}_3)_2\text{COO} + \text{SO}_2$ reaction.²⁸ A high-pressure limit k_5 value of $(4.7 \pm 0.1) \times 10^{-13} \text{ cm}^3 \text{ molecule}^{-1} \text{ s}^{-1}$ and k_{-6}/k_7 ratio of $(3.7 \pm 1.4) \times 10^{16} \text{ molecule cm}^{-3}$ were obtained from the fit. The error estimates are 2σ values from the fit. Green and co-workers also observed a weak positive pressure dependence in the 4 to 50 Torr range using helium as a bath gas,¹⁷ and their value $k_5 = (3.5 \pm 0.8) \times 10^{-13} \text{ cm}^3 \text{ molecule}^{-1} \text{ s}^{-1}$ at 298 K and with 50 Torr (He) is in quantitative agreement with

our k_5 value of $(3.7 \pm 0.25) \times 10^{-13} \text{ cm}^3 \text{ molecule}^{-1} \text{ s}^{-1}$ at 301 K and 30 Torr (N_2), as shown in Figure 3. Taatjes and co-workers reported $k_5 = (2.3 \pm 0.3) \times 10^{-13} \text{ cm}^3 \text{ molecule}^{-1} \text{ s}^{-1}$ at 293 K and in 4 Torr of helium, whereas extrapolation of the fitted function obtained from Figure 2 to a pressure of 4 Torr gives a k_5 value from our work of $(3.7 \pm 0.4) \times 10^{-13} \text{ cm}^3 \text{ molecule}^{-1} \text{ s}^{-1}$. This comparison suggests an activation or stabilization of intermediates involved in the reaction pathway, and that the reaction reaches the high-pressure limit at lower total pressure when N_2 is used as a bath gas instead of He. Dependence of the reaction rate on pressure and the nature of the bath gas has been reported previously for the reaction of $(\text{CH}_3)_2\text{CO}$ with SO_2 .^{27, 28} The $(\text{CH}_3)_2\text{CO} + \text{SO}_2$ and $\text{CH}_2\text{OO} + (\text{CH}_3)_2\text{CO}$ reactions are predicted to follow similar cycloaddition pathways,²⁹⁻³¹ which might cause comparable collisional activation or stabilization behaviour.

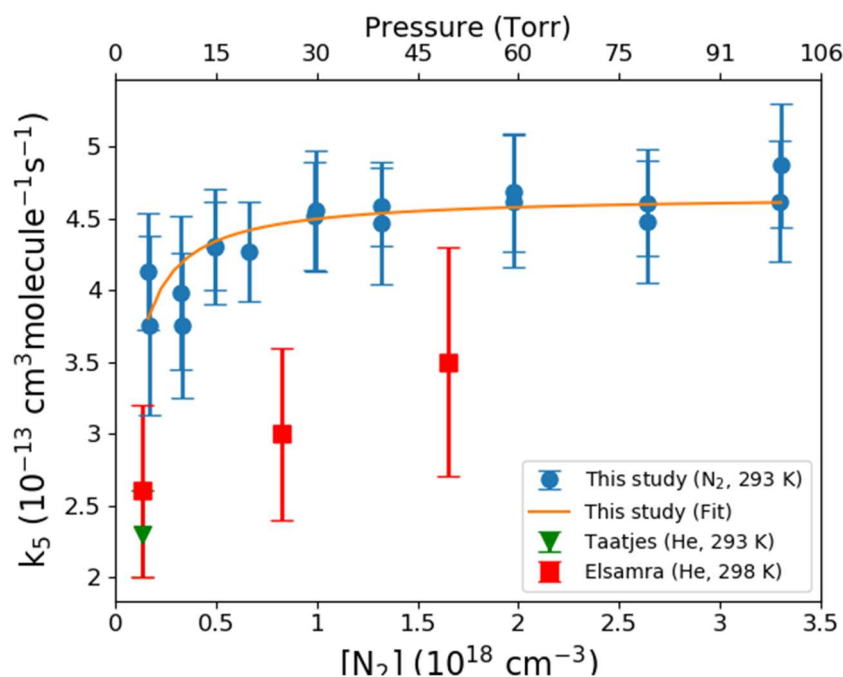


Figure 2. Rate coefficient for the $\text{CH}_2\text{OO} + (\text{CH}_3)_2\text{CO}$ reaction as a function of N_2 bath gas pressure at 293 K. The error bars represent a combination of systematic and statistical uncertainties, as is described in the text. Rate coefficients reported by Taatjes *et al.*¹⁶ and Elsamra *et al.*¹⁷ are included for comparison.

The k_5 values were measured over a range of temperatures relevant in the troposphere at fixed bath gas (N_2) pressures of 30 and 60 Torr, with the outcomes shown in Figure 3. According to the analysis summarized in Figure 2, the reaction is expected to be in the high pressure limit at both of these pressures, and k_5 values for both pressures show similar negative temperature dependence. The k_5 values increase by about a factor of 5 as the temperature reduces from 310 to 250 K. The rate coefficient values are provided in Tables S2 (30 Torr) and S3 (60 Torr) in the supporting information. In the high pressure limit, the kinetic model used for pressure stabilization (reactions (R6) – (R8)) reduces to a system of pre-reaction equilibrium between reactants and a thermalised complex, followed by unimolecular reaction over an energy barrier:



Applying the steady state approximation to the concentration of the pre-reactive complex, assuming complex dissociation is faster than reaction over the barrier (i.e., $k_9 \gg k_{10}$), and using statistical thermodynamics and transition state theory arguments, the reaction rate can be expressed as:

$$k(T) = AT^2 \exp\left(-\frac{\Delta H}{RT}\right) \quad (E5)$$

Here, A and ΔH are given by:

$$A = \frac{R'k_B}{N_A h} \exp\left(\frac{\Delta S_9 + \Delta S_{10}}{R}\right) \quad (E6)$$

$$\Delta H = \Delta H_9 + \Delta H_{10} \quad (E7)$$

In Equations (E5 – E7), R' and R denote the molar gas constant in different units ($R' = 82.1 \text{ cm}^3 \text{ atm mol}^{-1} \text{ K}^{-1}$ and $R = 8.31 \text{ J mol}^{-1} \text{ K}^{-1}$), N_A is the Avogadro constant, k_B is the Boltzmann constant, and T is the absolute temperature. ΔS_{10} and ΔH_{10} are, respectively, the entropy and enthalpy changes for activation of the pre-reactive complex to the transition state for product formation via reaction (R10). Similarly, ΔS_9 and ΔH_9 are the changes in entropy and enthalpy for the complexation step, (R9). A derivation of equation (E5) is provided in our previous study.¹⁴ The quality of the fit is good, as shown by the green line in Figure 3, and returns fitted values of $A = (1.4 \pm 0.2) \times 10^{-21} \text{ cm}^3 \text{ molecule}^{-1} \text{ s}^{-1} \text{ K}^{-2}$ and $\Delta H = -20.1 \pm 0.3 \text{ kJ mol}^{-1}$. Figure 3 also shows that an extrapolation of the fitted curve to 500 K gives good agreement with the measured rate coefficient values reported by Elsamra *et al.*¹⁷ The $\Delta H = -20.0 \pm 0.3 \text{ kJ mol}^{-1}$ value is in good agreement with the previously reported computational barrier height of $-20.5 \text{ kJ mol}^{-1}$.³¹ However, this agreement between the enthalpy change and barrier height may be fortuitous as recent master equation calculations of Criegee intermediate reactions with NH_3

and CH_3NH_2 , which have energetics similar to reaction with acetone, showed that these reactions were not in thermal equilibrium at ambient conditions.³²

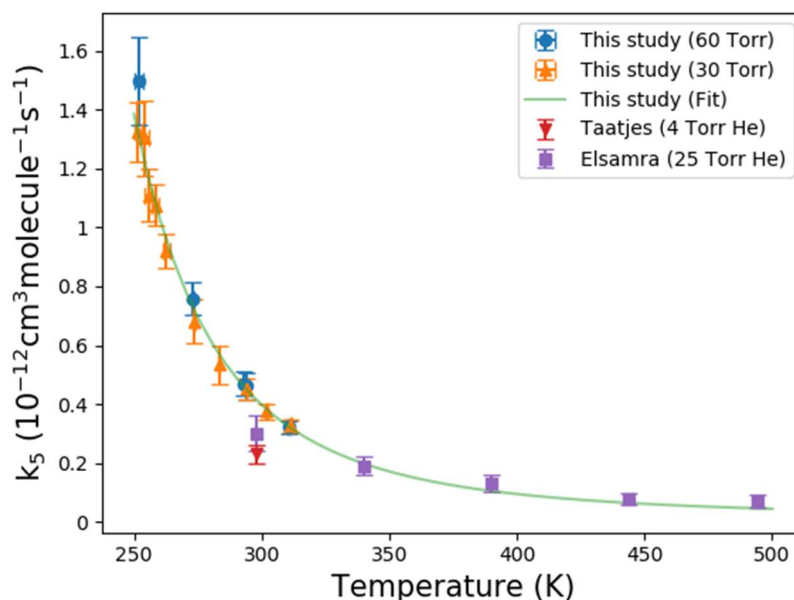


Figure 3. Temperature dependence of the k_5 values measured at 30 Torr (orange triangles) and 60 Torr (blue circles) bath (N_2) gas pressures. The error bars represent a combination of systematic and statistical uncertainties, as is described in the text. The green line is a fit to the 30 and 60 Torr data sets from this work at temperatures from 250 – 310 K, obtained using the kinetic fitting model described in the text. The fit curve is extrapolated to 500 K for comparison with rate coefficient values measured by Elsamra *et al.* (purple squares).¹⁷ A comparison is also made to the rate coefficient reported by Taatjes *et al.* (dark red triangle) at 293 K and 4 Torr (He).¹⁶

3.2. Master Equation Modelling of the $\text{CH}_2\text{OO} + (\text{CH}_3)_2\text{CO}$ reaction. The observable rate coefficients for the $\text{CH}_2\text{OO} + (\text{CH}_3)_2\text{CO}$ reaction as a function of temperature and pressure were calculated using RRKM/ME simulations as described in Elsamra *et al.*¹⁷ Briefly, the

reaction is predicted to proceed by formation of a van der Waals complex before passing over a submerged barrier to form a secondary ozonide as shown in Figure 4. Only one cycloaddition pathway is possible because of the symmetric substitution of the carbonyl carbon atoms in both reactants. The molecular geometries and energies, calculated by Jalan *et al.*³¹ using RCCSD(T)-F12a/VTZ-F12//B3LYP/MG3S methods, were input to Arkane, a 1-D ME solver previously named Cantherm that is part of the RMG-Py package.³³ The $k(T,P)$ values output by Arkane that connect each minimum on the reaction pathway to every other minimum were used to calculate $k_{\text{obs}}(T,p)$ by applying the pseudo-steady-state approximation to the short-lived van der Waals (vdW) complex at the entrance of the reaction pathway. Arkane also requires as an input the high-pressure limit rate coefficient for the barrierless entrance channel forming the vdW complex. All the calculations were performed using the collisional energy transfer parameters for nitrogen bath gas used by Jalan *et al.*,³¹ which gave negligibly different results from a He bath gas at the experimental conditions of Elsamra *et al.*¹⁷ and Taatjes *et al.*¹⁶

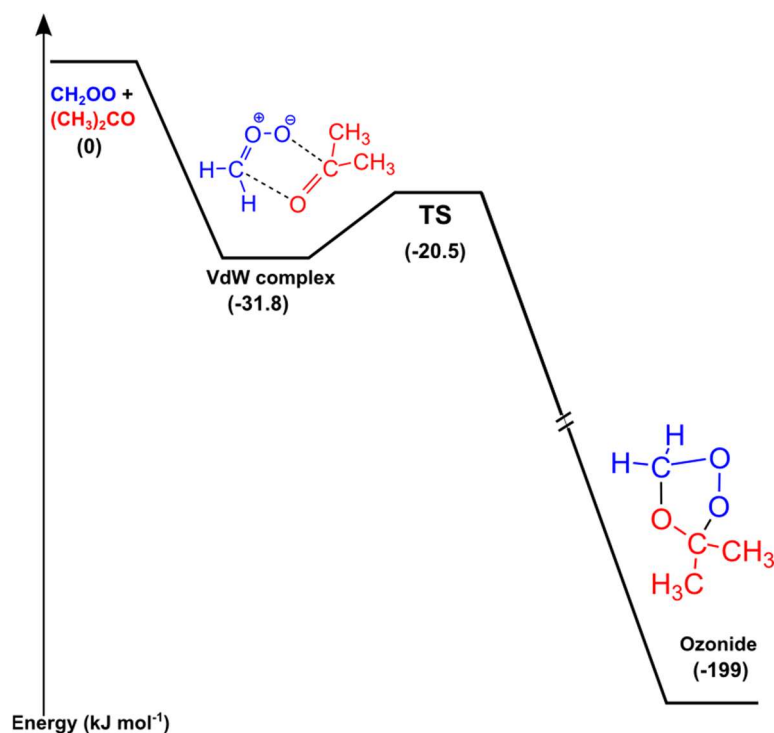


Figure 4. Minimum energy pathway for reaction of CH_2OO with $(\text{CH}_3)_2\text{CO}$. The stationary point energies were calculated at the RCCSD(T)-F12a/VTZ-F12//B3LYP/MG3S level of theory and were obtained from the previous study by Jalan *et al.*³¹

Figure 5 compares the experimentally observed rate coefficients with the calculated values using two different barrierless entrance rate coefficients: $6.6 \times 10^{-10} \text{ cm}^3 \text{ molecule}^{-1} \text{ s}^{-1}$ (ME I) and $1.3 \times 10^{-12} \text{ cm}^3 \text{ molecule}^{-1} \text{ s}^{-1}$ (ME II). The latter value was found by Jalan *et al.* to match the experiments of Taatjes *et al.* at 4 Torr and 298 K,³¹ but does not reproduce well the temperature-dependence measured here. The former value was estimated by Elsamra *et al.* using the method of Georgievskii and Klippenstein.^{17, 34} Additionally, the barrier height for the submerged inner transition state (TS) connecting the vdW complex to the stabilized products on the reaction pathway was varied by $\pm 2.9 \text{ kJ mol}^{-1}$ from an initial computed value of $-20.5 \text{ kJ mol}^{-1}$ with respect to the energy of separated reactants (as shown in figure 4). The initial computed barrier height value also included zero-point corrections. Raising the submerged barrier by 2.9 kJ mol^{-1} in combination with the barrierless entrance rate of $6.6 \times 10^{-$

$10 \text{ cm}^3 \text{ molecule}^{-1} \text{ s}^{-1}$ gave closest agreement with the experimental rate coefficients across the entire temperature range of 250-500 K. A barrier height error of around 4.2 kJ mol^{-1} would be within the uncertainties expected for quantum chemistry calculations. However, the curvature of the experimentally measured T-dependence is not replicated by the ME simulations, which might be due to the omission of any T-dependence to the estimated barrierless entrance rate, but further analysis is beyond the scope of the current study.

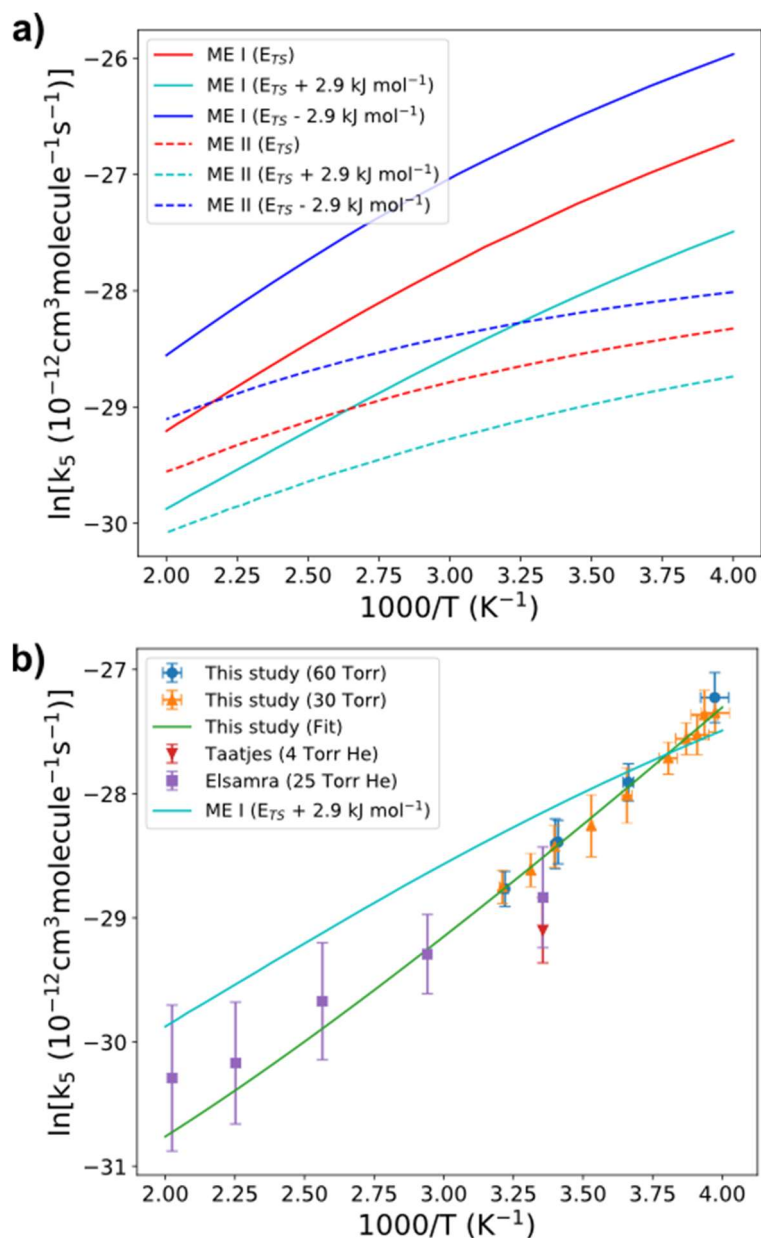


Figure 5. a) Master equation simulations using entrance rate coefficient values of 6.6×10^{-10} (MEI) and $1.3 \times 10^{-12} \text{ cm}^3 \text{ molecule}^{-1} \text{ s}^{-1}$ (MEII). Both calculations were performed using various barrier heights for the inner transition state, as explained in the text. b) Comparison of the experimental and best master equation simulated rate coefficients. The green solid line is the fit obtained using the kinetic model described in the text.

4. Atmospheric Implications

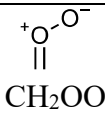
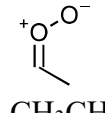
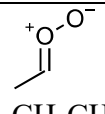
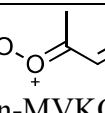
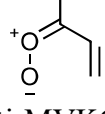
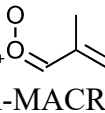
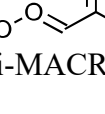
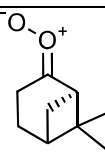
4.1. Global Modelling of Criegee Intermediates. To assess the atmospheric implications of our measured reaction rates, we compare the removal of tropospheric acetone by Criegee intermediates to its removal by reaction with OH radicals, photolysis and dry deposition using a 3-D global chemistry transport model, STOCHEM-CRI. A steady state speciated Criegee intermediate field was generated previously using modelled alkene and ozone concentrations, and Criegee intermediate losses by unimolecular reaction and reaction with water or water dimers.³⁵ In the current study, all the production and sink reactions of Criegee intermediates were fully integrated in the model. In addition to ethene, propene, E-2-butene, isoprene, α -pinene and β -pinene, three further alkenes, methacrolein (MACR), methyl vinyl ketone (MVK) and 4-hydroxy-2-methyl-2-butenal (HC4CCHO), were included in the current model. The new alkenes added in the model are produced during oxidation of isoprene in the troposphere. The labels in parenthesis are those used in Master Chemical Mechanism scheme.³⁶ The rate coefficients for the Criegee intermediate loss processes were updated with recently reported temperature-dependent rate coefficients and are shown in Table 1 for the Criegee intermediates considered in the model chemistry. The rate coefficient expressions for CH₂OO and anti-CH₃CHOO reactions were obtained from direct time resolved kinetic studies by Lin and co-workers,^{37, 38} while those for syn-CH₃CHOO, syn-MVKOO (E-(CH=CH₂)(CH₃)COO) and anti-MVKOO (Z-(CH=CH₂)(CH₃)COO) were obtained from the combined microcanonical kinetic rate measurements and theoretical studies by Lester and co-workers.^{10, 39} The rate expressions for anti-nopinone oxide (E-pinone oxide), syn-pinonaldehyde oxide (Z-pinonaldehyde A oxide), anti-isopinonaldehyde oxide (E-pinonaldehyde K oxide) and anti-(CH₃)(CHO)COO (E-(CHO)(CH₃)COO) were assumed to be the same as for syn-CH₃CHOO (Z-CH₃CHOO), because of the similarities in their structures. Likewise, the rate expression for anti-pinonaldehyde oxide (E-pinonaldehyde oxide) and anti-CH₃C(O)CHOO (Z-(CHO)(CH₃)COO) were taken to be same as for anti-CH₃CHOO (E-CH₃CHOO). The

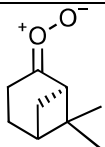
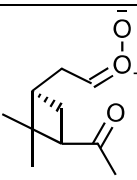
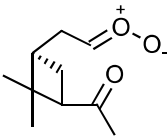
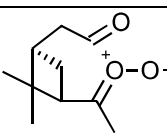
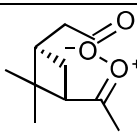
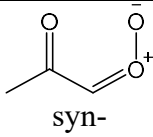
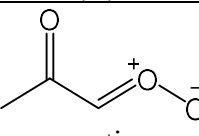
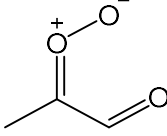
theoretical study of Vereecken *et al.* provided the rate expressions used for syn-MACROO (Z-C(CH₃)=CH₂)CHOO), anti-MACROO (E-C(CH₃)=CH₂)CHOO), syn-nopinone oxide (Z-pinone oxide), syn-isopinonealdehyde oxide (Z-pinonaldehyde K oxide), syn-CH₃C(O)CHOO (Z-C(O)CH₃CHOO) and syn-(CH₃)(CHO)COO (Z-(CHO)(CH₃)COO) because the structures of these species differ significantly from the simpler Criegee intermediates studied in direct laboratory measurements.⁹ The labels in parenthesis are those used by Vereecken *et al.* for the various Criegee intermediates.⁹ The hydroxy substituted Criegee intermediates possible from ozonolysis of HC₄CCHO are not included in the model as the chemistry of these Criegee intermediates is not yet well studied. The calculation of the speciated Criegee intermediates yield from ozonolysis of various alkenes incorporated in the updated STOCHEM-CRI model are described in our previous publication.³⁵ The yields of stabilised Criegee intermediates from the ozonolysis of MACR, MVK and HC₄CCHO were taken from the MCM website.³⁶

Figure 6 shows the surface and zonal plots of the updated annual global integrated Criegee intermediate field. The ground and upper troposphere surface plots are generated by vertically integrating the pressure range from 1013 to 912 hPa and 302.9 to 201.4 hPa, respectively, whereas the zonal plots are obtained by horizontally integrating the global surface. An integrated global burden of 41 kg per year is estimated for all the Criegee intermediates and Table 1 shows the percent contribution of the various Criegee intermediates used in the model. Syn-MVKOO and anti-MACROO form the largest fraction of the integrated Criegee intermediate field, with around 50 and 9.5 percent of total global Criegee intermediate burden by weight, respectively. Larger Criegee intermediates such as syn-MVKOO and anti-MACROO, with slow unimolecular reactions and slow reactions with H₂O, are present in abundance in the ground surface layer, whereas CH₂OO is the main contributor in the upper troposphere as shown in Figure 6. The upper troposphere has much lower H₂O concentrations

and thus the sink reaction of CH₂OO with water is less important. CH₂OO can also be formed from the ozonolysis of fragments of isoprene ozonolysis, resulting in long range transport. The unimolecular decomposition of CH₂OO is predicted to be slow ($\leq 0.001 \text{ s}^{-1}$) and thus was not included in the model.⁴⁰ The northern hemisphere has lower Criegee intermediate concentrations because of higher seasonal fluctuations of the alkene emissions, as is shown in Figure S1 in the Supporting Information. Alkene emissions in the tropical regions, mainly comprising isoprene, are larger, with minimal seasonal fluctuations, resulting in higher Criegee intermediate concentrations. The temperate region is richer in larger Criegee intermediates than the tropical region because of greater pinene emissions. The highest annual integrated Criegee intermediate concentrations of around $10^4 \text{ molecule cm}^{-3}$ are predicted in the Amazon region, which is lower than reported in our previous study by an order of magnitude.³⁵ This difference arises because of the updated loss reactions for the larger Criegee intermediates formed from ozonolysis of isoprene and pinenes. The updated model Criegee intermediate field in the tropical region is in good agreement with the prediction by Vereecken *et al.*⁹, but the temperate region Criegee intermediate annual average concentration is smaller than their prediction, most likely because of the smaller terpene emission inventory used in STOCHEM-CRI. However, the predicted summer time average concentration of up to $1000 \text{ molecule cm}^{-3}$ in the boreal region, shown in Figure S1a in the Supporting Information, is within the lower bound of the estimate provided by Novelli *et al.* using FAGE measurements.⁴¹

Table 1. Various Criegee intermediates incorporated in the STOCHEM-CRI model, the rate coefficients for their major sinks in the troposphere, and their percent contribution to the total Criegee intermediate global burden of 41 kg per year.

Criegee Intermediate	Alkenes (Criegee yield)	Major Criegee Intermediate Sinks (units of k_{uni} and $k_{\text{H}_2\text{O}}/k_{(\text{H}_2\text{O})_2}$ are s^{-1} and $\text{cm}^3 \text{molecule}^{-1} \text{s}^{-1}$, respectively)	Percent Contribution
 CH_2OO	Ethene (0.37) ⁴² Propene (0.37) ⁴² Isoprene (0.31) ⁴³ β -pinene (0.17) ⁴⁴ MVK (0.12) ³⁶ MACR (0.33) ³⁶	$k_{(\text{H}_2\text{O})_2}$: $3.92 \times 10^{-16} \exp(2930/T)$ [Ref. 37]	19.0
 $\text{syn-CH}_3\text{CHOO}$	Propene (0.08) ⁴² E-2-Butene (0.105) ^{45, 46}	k_{uni} : $2.76 \times 10^{-73} T^{27.88} \exp(3978/T)$ [Ref. 39]	0.9
 $\text{anti-CH}_3\text{CHOO}$	Propene (0.08) ⁴² E-2-Butene (0.105) ^{45, 46}	$k_{\text{H}_2\text{O}}$: 1.3×10^{-14} $k_{(\text{H}_2\text{O})_2}$: $5.23 \times 10^{-20} \exp(6124/T)$ [Ref. 47]	0.1
 syn-MVKOO	Isoprene (0.14) ⁴³	k_{uni} : $2.46 \times 10^{-76} T^{29.09} \exp(3545/T)$ [Ref. 10]	49.8
 anti-MVKOO	Isoprene (0.07) ⁴³	k_{uni} : $1.94 \times 10^{12} \exp(-6150/T)$ [Ref. 10]	1.1
 syn-MACROO	Isoprene (0.01) ⁴³	k_{uni} : $1.59 \times 10^{11} T^{0.44} \exp(-6102/T)$ [Ref. 9]	0.2
 anti-MACROO	Isoprene (0.04) ⁴³	k_{uni} : $5.93 \times 10^8 T^{1.46} \exp(-7832/T)$ $k_{\text{H}_2\text{O}}$: $2.13 \times 10^{-19} T^{1.74} \exp(-929/T)$ $k_{(\text{H}_2\text{O})_2}$: $2.24 \times 10^{-19} T^{1.73} \exp(1313/T)$ [Ref. 9]	9.5
 $\text{anti-nopinone oxide}$	β -pinene (0.18) ⁴⁴	k_{uni} : $2.76 \times 10^{-73} T^{27.88} \exp(3978/T)$ [same as $\text{syn-CH}_3\text{CHOO}$]	0.1

 <p>syn-nopinone oxide</p>	β -pinene (0.02) ⁴⁴	$k_{\text{uni}}: 1.9 \times 10^9 T^{1.33} \exp(-8425/T)$ $k_{\text{H}_2\text{O}}: 8.46 \times 10^{-23} T^{2.64} \exp(121/T)$ [Ref. 9]	1.8
 <p>syn- pinonaldehyde oxide</p>	α -pinene (0.05) ⁴⁸	$k_{\text{uni}}: 2.76 \times 10^{-73} T^{27.88} \exp(3978/T)$ [same as syn-CH ₃ CHOO]	2.1
 <p>anti- pinonaldehyde oxide</p>	α -pinene (0.05) ⁴⁸	$k_{\text{H}_2\text{O}}: 1.3 \times 10^{-14}$ $k_{(\text{H}_2\text{O})_2}: 5.23 \times 10^{-20} \exp(6124/T)$ [same as anti-CH ₃ CHOO]	0.2
 <p>anti- isopinonaldehyde oxide</p>	α -pinene (0.05) ⁴⁸	$k_{\text{uni}}: 2.76 \times 10^{-73} T^{27.88} \exp(3978/T)$ [same as syn-CH ₃ CHOO]	1.9
 <p>syn- isopinonaldehyde oxide</p>	α -pinene (0.05) ⁴⁸	$k_{\text{uni}}: 6.95 \times 10^{-66} T^{25.7} \exp(2391/T)$ [Ref. 9]	4.2
 <p>syn- CH₃C(O)CHOO</p>	MVK (0.06) ³⁶	$k_{\text{H}_2\text{O}}: 2.18 \times 10^{-19} T^{1.43} \exp(1268/T)$ $k_{(\text{H}_2\text{O})_2}: 2.26 \times 10^{-19} T^{1.43} \exp(3279/T)$ [Ref. 9]	4.9
 <p>anti- CH₃C(O)CHOO</p>	MVK (0.06) ³⁶	$k_{\text{H}_2\text{O}}: 1.3 \times 10^{-14} \text{ cm}^3 \text{ molecule}^{-1} \text{ s}^{-1}$ $k_{(\text{H}_2\text{O})_2}: 5.23 \times 10^{-20} \exp(6124/T)$ [same as anti-CH ₃ CHOO]	0.1
 <p>syn- (CH₃)(CHO)COO</p>	MACR (0.01) ³⁶ HC4CCHO (0.025) ³⁶	$k_{\text{uni}}: 2.76 \times 10^{10} T^{0.78} \exp(-5162/T)$ $k_{\text{H}_2\text{O}}: 7.81 \times 10^{-20} T^{1.68} \exp(757/T)$ $k_{(\text{H}_2\text{O})_2}: 8.07 \times 10^{-20} T^{1.67} \exp(2828/T)$ [Ref. 9]	3.9

anti- (CH ₃)(CHO)COO	MACR (0.01) ³⁶ HC4CCHO (0.025) ³⁶	$k_{\text{uni}}: 2.76 \times 10^{-73} T^{27.88} \exp(3978/T)$ [same as syn-CH ₃ CHOO]	0.2
-------------------------------------	---	---	-----

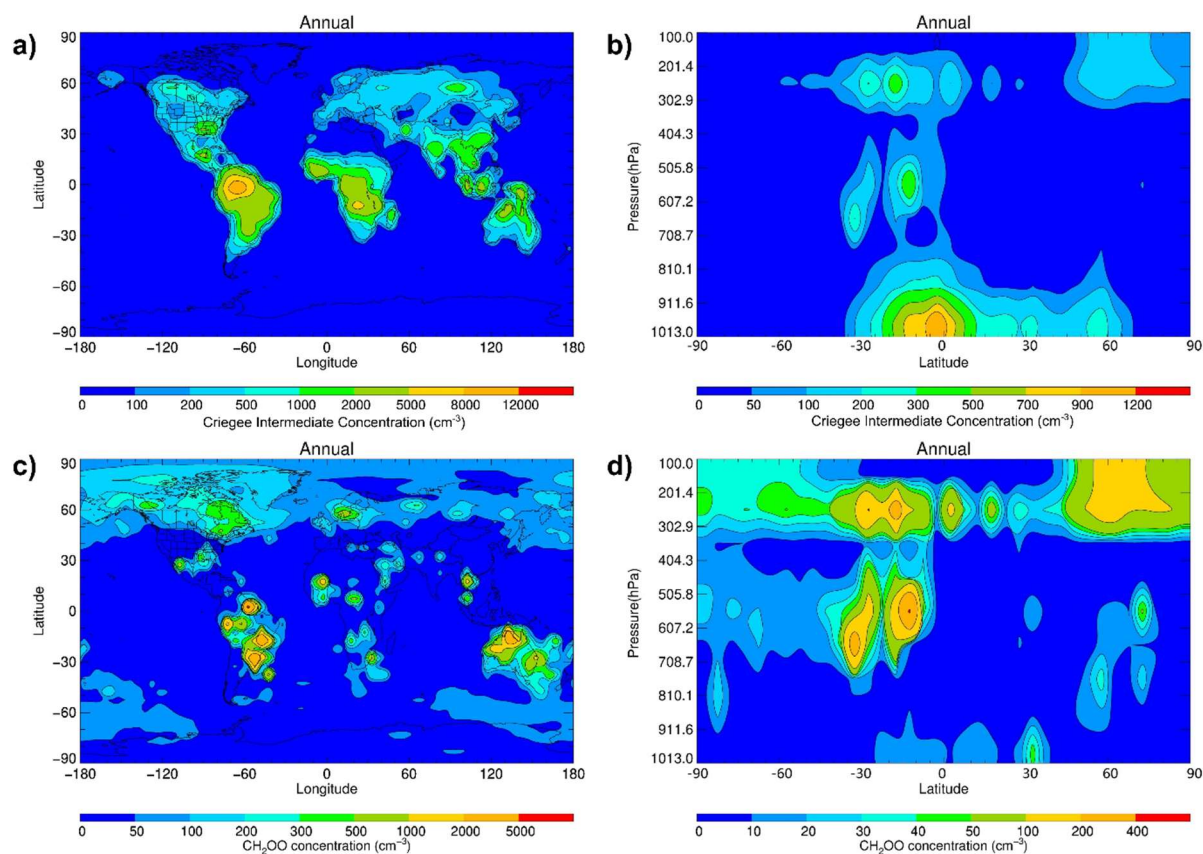


Figure 6. a) Ground surface and b) zonal annual average global concentration of all Criegee intermediates shown in Table 1 and c) upper troposphere surface and d) zonal average global concentration of CH₂OO obtained from the STOCHEM-CRI model described in the text.

4.2. Global Modelling of Acetone Reaction with Criegee Intermediates. The updated Criegee intermediate field and the temperature dependent rate coefficients for Criegee intermediate reactions (Table 1) were coupled with the acetone field reported previously by Khan *et al.*¹ to quantify the effect of reactive loss by Criegee intermediates on acetone

concentrations. The acetone sources in the model included direct emission, oxidation of propane and degradation of monoterpenes. The acetone sinks in the model included reaction with OH radicals, photolysis and dry deposition. Figure S2 in the supporting information shows the annual average acetone field, and concentrations of up to 2 ppb are predicted in various regions of the globe. Figure 7 shows the modelled change in acetone concentration after inclusion of reaction with Criegee intermediates. All the Criegee intermediates were assumed to react with mechanisms similar to that for CH₂OO with acetone. Figure 7a shows the annual surface plot of the change in acetone concentration obtained by vertical integration of the zonal plot shown in Figure 7b in the pressure range from 1013 to 912 hPa. Up to 40 ppt loss is estimated in equatorial regions where there is significant co-location between the Criegee intermediate and acetone fields. The tropical rainforests emit large amounts of alkenes to the atmosphere, producing Criegee intermediates which enhance acetone loss. Figure 7b shows a zonal plot of the loss in annual acetone concentration obtained from horizontal integration of the global surface. The temperate region shows the largest average loss in acetone concentration, mainly because of the greater land mass in this region with associated alkene emissions. The predicted acetone loss does not change significantly with altitude because of the negative temperature dependence of the rate coefficients for Criegee intermediate reactions with acetone. The rate coefficients for reaction of acetone with OH radicals vary from $(1.3 - 2.4) \times 10^{-13} \text{ cm}^3 \text{ molecule}^{-1} \text{ s}^{-1}$ in the 250 K to 310 K range, and thus are lower than for reaction with CH₂OO (see Figure 3). However, the concentration of OH radicals is significantly larger than the combined concentrations of CH₂OO and all other troposphericly active Criegee intermediates. Overall, the updated model predicts global acetone removal contributions by Criegee intermediates to be less than 1%, compared to 42% each by OH radical reaction and photolysis, and 16% by dry deposition. The rates of reaction of acetone with different Criegee intermediates may depend on the structure of the Criegee

intermediates and incorporation of this variability into the model may change their predicted contributions towards the global sinks of acetone. The ozonide adducts are predicted to be relatively volatile with vapour pressures > 0.002 Torr, using the method described in our previous study for the case of ester adducts,¹⁵ and thus are not likely to contribute to secondary organic aerosol formation.

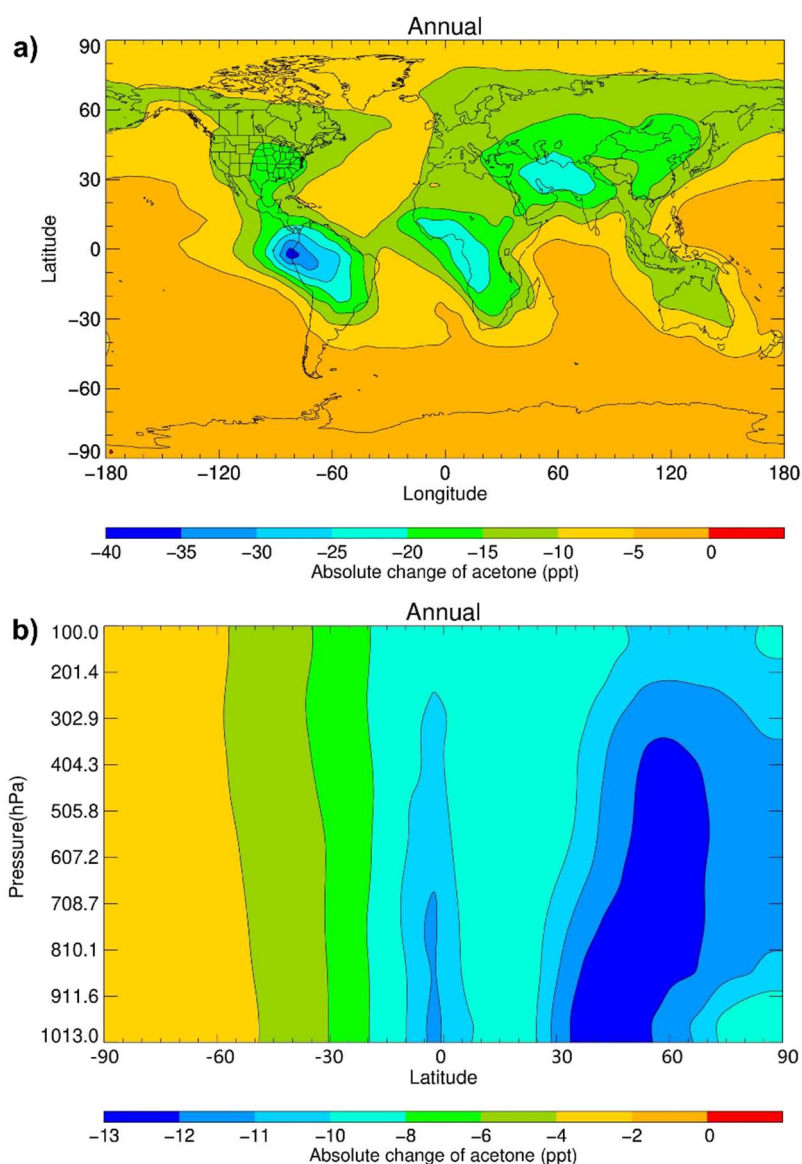


Figure 7. a) Surface and b) zonal plots of the change in annual acetone concentration after inclusion of loss reaction with Criegee intermediates, obtained using the STOCHEM-CRI model described in Ref 1.

5. Conclusions

Reaction rates of the simplest Criegee intermediate CH_2OO with acetone were measured at various pressures and temperatures relevant in the troposphere. The reaction rate coefficients show a small positive pressure dependence and a negative temperature dependence. An updated chemical reaction scheme was used to generate a speciated Criegee intermediate field in a global atmospheric and chemistry transport model which was then coupled with an acetone field with the newly measured rate coefficient values. The model outputs predict that these reactions are estimated to contribute to loss of up to 40 ppt of acetone in the troposphere.

ASSOCIATED CONTENT

Supporting Information. Rate coefficients for $\text{CH}_2\text{OO} + (\text{CH}_3)_2\text{CO}$ reaction as function of pressure (Table S1) and temperature (Table S2 and S3), seasonal average concentration of Criegee intermediates (Figure S1) and annual average zonal and surface concentrations of acetone (Figure S2).

AUTHOR INFORMATION

Corresponding Authors

*rcpchem@gmail.com

*a.orr-ewing@bristol.ac.uk

Note

The authors declare no competing financial interest. Experimental data and analysis scripts are archived in the University of Bristol's Research Data Storage Facility (DOI: 10.5523/bris.udkszetrifdl2f3aztxw1da4r)

ACKNOWLEDGMENTS

This research was funded by the Natural Environment Research Council (NERC grants NE/K004905/1 and NE/P013104/1). The research was carried out in part by the Jet Propulsion Laboratory, California Institute of Technology, under contract with the National Aeronautics and Space Administration (NASA), supported by the Upper Atmosphere Research and Tropospheric Chemistry program. We thank Prof. William H. Green (MIT) for helpful discussions.

REFERENCES

1. Khan, M. A. H.; Cooke, M. C.; Utembe, S. R.; Archibald, A. T.; Maxwell, P.; Morris, W. C.; Xiao, P.; Derwent, R. G.; Jenkin, M. E.; Percival, C. J.; Walsh, R. C.; Young, T. D. S.; Simmonds, P. G.; Nickless, G.; O'Doherty, S.; Shallcross, D. E., A Study of Global Atmospheric Budget and Distribution of Acetone using Global Atmospheric Model STOCHEM-CRI. *Atmos. Environ.* **2015**, *112*, 269-277.
2. Singh, H. B.; Kanakidou, M.; Crutzen, P. J.; Jacob, D. J., High Concentrations and Photochemical Fate of Oxygenated Hydrocarbons in the Global Troposphere. *Nature* **1995**, *378*, 50-54.
3. Jacob, D. J.; Field, B. D.; Jin, E. M.; Bey, I.; Li, Q.; Logan, J. A.; Yantosca, R. M.; Singh, H. B., Atmospheric Budget of Acetone. *J. Geophys. Res.* **2002**, *107*, 4100.
4. Gierczak, T.; Burkholder, J. B.; Bauerle, S.; Ravishankara, A. R., Photochemistry of Acetone under Tropospheric Conditions. *Chem. Phys.* **1998**, *231*, 229-244.
5. Arnold, S. R.; Chipperfield, M. P.; Blitz, M. A., A Three-Dimensional Model Study of the Effect of New Temperature-Dependent Quantum Yields for Acetone Photolysis. *J. Geophys. Res.* **2005**, *110*, D22305.
6. Johnson, D.; Martson, G., The Gas-Phase Ozonolysis of Unsaturated Volatile Organic Compounds in the Troposphere. *Chem. Soc. Rev.* **2008**, *37*, 699-716.
7. Taatjes, C. A., Criegee Intermediates: What Direct Production and Detection Can Teach Us About the Reactions of Carboxyl oxides. *Annu. Rev. Phys. Chem.* **2017**, *68*, 183-207.
8. Lin, J. J.-M.; Chao, W., Structure-Dependent Reactivity of Criegee Intermediates Studied with Spectroscopic Methods. *Chem. Soc. Rev.* **2017**, *46*, 7483-7497.
9. Vereecken, L.; Novelli, A.; Taraborrelli, D., Unimolecular Decay Strongly Limits the Atmospheric Impact of Criegee Intermediates. *Phys. Chem. Chem. Phys.* **2017**, *19*, 31599-31612.
10. Barber, V. P.; Pandit, S.; Green, A. M.; Trongsirivat, N.; Walsh, P. J.; Klippenstein, S. J.; Lester, M. I., Four Carbon Criegee Intermediate from Isoprene Ozonolysis: Methyl Vinyl Ketone Oxide Synthesis, Infrared Spectrum, and OH Production. *J. Am. Chem. Soc.* **2018**, *140*, 10866-10880.
11. Taatjes, C. A.; Welz, O.; Eskola, A. J.; Savee, J. D.; Scheer, A. M.; Shallcross, D. E.; Rotavera, B.; Lee, E. P. F.; Dyke, J. M.; Mok, D. K. W.; Osborn, D. L.; Percival, C. J.,

- Direct Measurements of Conformer-Dependent Reactivity of the Criegee Intermediate CH_3CHOO . *Science* **2013**, *340*, 177-180.
12. Percival, C. J.; Welz, O.; Eskola, A. J.; Savee, J. D.; Osborn, D. L.; Topping, D. O.; Lowe, D.; Utembe, S. R.; Bacak, A.; McFiggans, G.; Cooke, M. C.; Xiao, P.; Archibald, A. T.; Jenkin, M. E.; Derwent, R. G.; Riipinen, I.; Mok, D. W. K.; Lee, E. P. F.; Dyke, J. M.; Taatjes, C. A.; Shallcross, D. E., Regional and Global Impacts of Criegee Intermediates on Atmospheric Sulphuric Acid Concentrations and First Steps of Aerosol Formation. *Faraday Discuss.* **2013**, *165*, 45-73.
 13. Welz, O.; Eskola, A. J.; Sheps, L.; Rotavera, B.; Savee, J. D.; Scheer, A. M.; Osborn, D. L.; Lowe, D.; Booth, A. M.; Xiao, P.; Khan, M. A. H.; Percival, C. J.; Shallcross, D. E.; Taatjes, C. A., Rate Coefficients of C1 and C2 Criegee Intermediate Reactions with Formic and Acetic Acid Near the Collision Limit: Direct Kinetics Measurements and Atmospheric Implications. *Angew. Chem. Int. Ed.* **2014**, *53*, 4547-4550.
 14. Chhantyal-Pun, R.; McGillen, M. R.; Beames, J. M.; Khan, M. A.; Percival, C. J.; Shallcross, D. E.; Orr-Ewing, A. J., Temperature Dependence of the Rates of Reaction of Trifluoroacetic Acid with Criegee Intermediates. *Angew. Chem. Int. Ed.* **2017**, *56*, 9044-9047.
 15. Chhantyal-Pun, R.; Rotavera, B.; McGillen, M. R.; Khan, M. A. H.; Eskola, A. J.; Caravan, R. L.; Blacker, L.; Tew, D. P.; Osborn, D. L.; Percival, C. J.; Taatjes, C. A.; Shallcross, D. E.; Orr-Ewing, A. J., Criegee Intermediate Reactions with Carboxylic Acids: A Potential Source of Secondary Organic Aerosol in the Atmosphere. *ACS Earth Space Chem.* **2018**, *2*, 833-842.
 16. Taatjes, C. A.; Welz, O.; Eskola, A. J.; Savee, J. D.; Osborn, D. L.; Lee, E. P. F.; Dyke, J. M.; Mok, D. W. K.; Shallcross, D. E.; Percival, C. J., Direct Measurement of Criegee Intermediate (CH_2OO) Reactions with Acetone, Acetaldehyde, and Hexafluoroacetone. *Phys. Chem. Chem. Phys.* **2012**, *14*, 10391-10400.
 17. Elsamra, R. M. I.; Jalan, A.; Buras, Z. J.; Middaugh, J. E.; Green, W. H., Temperature- and Pressure-Dependent Kinetics of $\text{CH}_2\text{OO} + \text{CH}_3\text{COCH}_3$ and $\text{CH}_2\text{OO} + \text{CH}_3\text{CHO}$: Direct Measurements and Theoretical Analysis. *Int. J. Chem. Kinet.* **2016**, *48*, 474-488.
 18. Welz, O.; Savee, J. D.; Osborn, D. L.; Vasu, S. S.; Percival, C. J.; Shallcross, D. E.; Taatjes, C. A., Direct Kinetic Measurements of Criegee Intermediate (CH_2OO) Formed by Reaction of CH_2I with O_2 . *Science* **2012**, *335*, 204-207.
 19. Chhantyal-Pun, R.; Davey, A.; Shallcross, D. E.; Percival, C. J.; Orr-Ewing, A. J., A Kinetic Study of the CH_2OO Criegee Intermediate Self-Reaction, Reaction with SO_2 and Unimolecular Reaction Using Cavity Ring-Down Spectroscopy. *Phys. Chem. Chem. Phys.* **2015**, *17*, 3617-3626.
 20. Collins, W. J.; Stevenson, D. S.; Johnson, C. E.; Derwent, R. G., The European Regional Ozone Distribution and Its Links with the Global Scale for the Years 1992 and 2015. *Atmos. Environ.* **2000**, *34*, 255-267.
 21. Derwent, R. G.; Collins, W. J.; Johnson, C. E.; Stevenson, D. S., Transient Behaviour of Tropospheric Ozone Precursors in a Global 3-D CTM and Their Indirect Greenhouse Effects. *Climate Change* **2001**, *49*, 463-487.
 22. Collins, W. J.; Stevenson, D. S.; Johnson, C. E.; Derwent, R. G., Tropospheric Ozone in a Global-Scale Three-Dimensional Lagrangian Model and Its Response to NO_x Emission Controls. *J. Atm. Chem.* **1997**, *26*, 223-274.
 23. Derwent, R. G.; Stevenson, D. S.; Doherty, R. M.; Collins, W. J.; Sanderson, M. G., How is Surface Ozone in Europe Linked to Asian and North American NO_x emissions? *Atmos. Environ.* **2008**, *42*, 7412-7422.

24. Jenkin, M. E.; Watson, L. A.; Utembe, S. R.; Shallcross, D. E., A Common Representative Intermediates (CRI) Mechanism for VOC degradation. Part 1: Gas Phase Mechanism Development. *Atmos. Environ.* **2008**, *42*, 7185-7195.
25. Watson, L. A.; Shallcross, D. E.; Utembe, S. R.; Jenkin, M. E., A Common Representative Intermediates (CRI) Mechanism for VOC Degradation. Part 2: Gas Phase Mechanism Reduction. *Atmos. Environ.* **2008**, *42*, 7196-7204.
26. Utembe, S. R.; Cooke, M. C.; Archibald, A. T.; Jenkin, M. E.; Derwent, R. G.; Shallcross, D. E., Using a Reduced Common Representative Intermediates (CRI v2-R5) Mechanism to Simulate Tropospheric Ozone in a 3-D Lagrangian Chemistry Transport Model. *Atmos. Environ.* **2010**, *13*, 1609-1622.
27. Chhantyal-Pun, R.; Welz, O.; Savee, J. D.; Eskola, A. J.; Lee, E. P. F.; Blacker, L.; Hill, H. R.; Ashcroft, M.; Khan, M. A. H.; Lloyd-Jones, G. C.; Evans, L.; Rotavera, B.; Huang, H.; Osborn, D. L.; Mok, D. K. W.; Dyke, J. M.; Shallcross, D. E.; Percival, C. J.; Orr-Ewing, A. J.; Taatjes, C. A., Direct Measurements of Unimolecular and Bimolecular Reaction Kinetics of the Criegee Intermediate (CH₃)₂COO. *J. Phys. Chem. A* **2017**, *121*, 4-15.
28. Huang, H.-L.; Chao, W.; Lin, J. J.-M., Kinetics of a Criegee Intermediate That Would Survive High Humidity and May Oxidize Atmospheric SO₂. *Proc. Natl. Acad. USA* **2015**, *112*, 10857-10862.
29. Kuwata, K. T.; Guinn, E. J.; Hermes, M. R.; Fernandez, J. A.; Mathison, J. M.; Huang, K., A Computational Re-examination of the Criegee Intermediate-Sulfur Dioxide Reaction. *J. Phys. Chem. A* **2015**, *119*, 10316-10335.
30. Vereecken, L.; Harder, H.; Novelli, A., The Reaction of Criegee Intermediates with NO, RO₂, and SO₂, and Their Fate in the Atmosphere. *Phys. Chem. Chem. Phys.* **2012**, *14*, 14682-14695.
31. Jalan, A.; Allenz, J. W.; Green, W. H., Chemically Activated Formation of Organic Acids in Reactions of the Criegee Intermediate with Aldehydes and Ketones. *Phys. Chem. Chem. Phys.* **2013**, *15*, 16841-16852.
32. Chhantyal-Pun, R.; Shannon, R. J.; Tew, D. P.; Caravan, R. L.; Duchi, M.; Wong, C.; Ingham, A.; Feldman, C.; McGillen, M. R.; Khan, M. A. H.; Antonov, I. O.; Rotavera, B.; Ramasesha, K.; Osborn, D. L.; Taatjes, C. A.; Percival, C. J.; Shallcross, D. E.; Orr-Ewing, A. J., Experimental and Computational Studies of Criegee Intermediate Reactions with NH₃ and CH₃NH₂. *Phys. Chem. Chem. Phys.* **2019**, *21*, 14042-14052.
33. Gao, C. W.; Allen, J. W.; Green, W. H.; West, R. H., Reaction Mechanism Generator: Automatic Construction of Chemical Kinetic Mechanisms. *Computer Physics Communications* **2016**, *203*, 212-225.
34. Georgievskii, Y.; Klippenstein, S. J., Long-Range Transition State Theory. *J. Chem. Phys.* **2005**, *122*, 194103.
35. McGillen, M. R.; Curchod, B. F. E.; Chhantyal-Pun, R.; Beames, J. M.; Watson, N.; Khan, M. A. H.; McMahon, L.; Shallcross, D. E.; Orr-Ewing, A. J., Criegee Intermediate-Alcohol Reactions, A Potential Source of Functionalized Hydroperoxides in the Atmosphere. *ACS Earth Space Chem.* **2017**, *1*, 664-672.
36. The Master Chemical Mechanism. <http://mcm.leeds.ac.uk/MCM> (accessed August 18, 2019).
37. Smith, M. C.; Chang, C.-H.; Chao, W.; Lin, L.-C.; Takahashi, K.; Boering, K. A.; Lin, J. J., Strong Negative Temperature Dependence of the Simplest Criegee Intermediate CH₂OO Reaction with Water Dimer. *J. Phys. Chem. Lett.* **2015**, *6*, 2708-2713.
38. Lin, L.-C.; Chang, H.-T.; Chang, C.-H.; Chao, W.; Smith, M. C.; Chang, C.-H.; Lin, J. J.-M.; Takahashi, K., Competition Between H₂O and (H₂O)₂ Reactions with CH₂OO/CH₃CHOO. *Phys. Chem. Chem. Phys.* **2016**, *18*, 4557-4568.

39. Fang, Y.; Liu, F.; Barber, V. P.; Klippenstein, S. J.; McCoy, A. B.; Lester, M. I., Communication: Real Time Observation of Unimolecular Decay of Criegee Intermediates to OH Radical Products. *J. Chem. Phys.* **2016**, *144*, 061102.
40. Stone, D.; Au, K.; Sime, S.; Medeiros, D. J.; Blitz, M.; Seakins, P. W.; Decker, Z.; Sheps, L., Unimolecular Decomposition Kinetics of the Stabilised Criegee Intermediates CH₂OO and CD₂OO. *Phys. Chem. Chem. Phys.* **2018**, *20*, 24940-24954.
41. Novelli, A.; Hens, K.; Ernest, C. T.; Martinez, M.; Nölscher, A. C.; Sinha, V.; Paasonen, P.; Petäjä, T.; Sipilä, M.; Elste, T.; Plass-Dülmer, C.; Phillips, G. J.; Kubistin, D.; Williams, J.; Vereecken, L.; Lelieveld, J.; Harder, H., Estimating the Atmospheric Concentration of Criegee Intermediates and Their Possible Interference in a FAGE-LIF Instrument. *Atmos. Chem. Phys.* **2017**, *17*, 7807-7826.
42. Atkinson, R.; Baulch, D. L.; Cox, R. A.; Crowley, J. N.; Hampson, R. F.; Hynes, R. G.; Jenkin, M. E.; Rossi, M. J.; Troe, J., Evaluated Kinetic and Photochemical Data for Atmospheric Chemistry: Volume II – Gas Phase Reactions of Organic Species. *Atmos. Chem. Phys.* **2006**, *6*, 3625-4035.
43. Zhang, D.; Lei, W.; Zhang, R., Mechanism of OH Formation From Ozonolysis of Isoprene: Kinetics and Product Yield. *Chem. Phys. Lett.* **2002**, *358*, 171-179.
44. Nguyen, T. L.; Peeters, J.; Vereecken, L., Theoretical Study of the Gas-Phase Ozonolysis of β -Pinene (C₁₀H₁₆). *Phys. Chem. Chem. Phys.* **2009**, *11*, 5643-5656.
45. Hasson, A. S.; Orzechowska, G.; Paulson, S. E., Production of Stabilized Criegee Intermediates and Peroxides in the Gas Phase Ozonolysis of Alkenes 1. Ethene, Trans-2-Butene, and 2,3-Dimethyl-2-Butene *J. Geophys. Res. Atmos.* **2001**, *106*, 34131-34142.
46. Hatakeyama, S.; Kobayashi, H.; Akimoto, H., Gas-Phase Oxidation of SO₂ in the Ozone-Olefin Reactions. *J. Phys. Chem.* **1984**, *88*, 4736-4739.
47. Lin, L.-C.; Chao, W.; Chang, C.-H.; Takahashi, K.; Lin, J. J.-M., Temperature Dependence of the Reaction of Anti-CH₃CHOO with Water Vapor. *Phys. Chem. Chem. Phys.* **2016**, *18*, 28189-28197.
48. Berndt, T.; Jokinen, T.; Mauldin, R. L.; Petäjä, T.; Herrmann, H.; Junninen, H.; Paasonen, P.; Worsnop, D. R.; Sipilä, M., Gas-Phase Ozonolysis of Selected Olefins: The Yield of Stabilized Criegee Intermediate and the Reactivity Toward SO₂. *J. Phys. Chem. Lett.* **2012**, *3*, 2892-2896.

TABLE OF CONTENTS GRAPHIC

